Hydride formation and stability on a Pd–SiO$_2$ thin-film model catalyst studied by TEM and SAED

Bernd Jenewein [a], Simon Penner [a,*], Harald Gabasch [a,b], Bernhard Klötzer [a], Di Wang [b],
Axel Knop-Gericke [b], Robert Schlögl [b], Konrad Hayek [a]

[a] *Institute of Physical Chemistry, University of Innsbruck, Innrain 52a, A-6020 Innsbruck, Austria*
[b] *Department of Inorganic Chemistry, Fritz-Haber-Institut of the Max-Planck Society, Faradayweg 4-6, D-14195 Berlin, Germany*

Abstract

Hydride formation was studied on Pd particles supported on SiO$_2$, and the results were evaluated with reference to a corresponding ZnO-promoted Pd/SiO$_2$ catalyst reported recently. Pd particles (mean size, ∼5 nm) were epitaxially grown on NaCl(001) cleavage faces and subsequently covered by a layer of amorphous SiO$_2$, thereby maintaining their epitaxial orientation. The films were subjected to various hydrogen and annealing treatments in the temperature regime of 373–873 K, and their stability in an O$_2$ environment (373–573 K) was also tested. The structural and morphological changes were followed by transmission electron microscopy and selected area electron diffraction. Reduction at 523 K increased the mean particle size considerably and converted the Pd particles into an amorphous hydride phase that decomposed at and above 673 K either by reduction in hydrogen or by annealing in He environment, forming a crystalline Pd$_2$Si phase. Oxidative treatments of the Pd–H phase at temperatures above 523 K induce transformation into partially *oriented* Pd particles. The Pd$_2$Si phase was stable under reductive conditions up to 873 K and decomposed into *disoriented* Pd particles on oxidation at temperatures at and above 573 K. Although the Pd/SiO$_2$ catalyst can be readily converted into an amorphous hydride phase, it loses its hydrogen storage capability on entering the silicide state at 673 K, and hence no hydride formation was observed. These results are in contrast to previous observations on a corresponding Pd/ZnO/SiO$_2$ catalyst, where the formation of a well-ordered PdZn alloy prevented the formation of the hydride phase and significantly enhanced the structural stability of the catalyst and its resistance against sintering. In contrast, the Pd/SiO$_2$ system was converted into the amorphous hydride state under "real" catalytic conditions, for example, during CO$_2$ hydrogenation at around 523 K.
© 2006 Elsevier Inc. All rights reserved.

Keywords: Hydride formation; Palladium; Silica; Electron microscopy; Selected area; Electron diffraction

1. Introduction

Knowledge of the interaction of hydrogen with metals and intermetallic compounds is not only of great interest due to the excellent hydrogen storage capabilities of many of these materials [1–9], but remains a key parameter especially in Pd-catalyzed reactions involving hydrogen. It is well known that Pd readily absorbs hydrogen in its crystal lattice even at low pressure and room temperature [10]. At low hydrogen concentrations, the α-phase is formed, usually considered a solid solution of hydrogen in the originally undistorted Pd lattice.

Once saturation of the hydrogen concentration in the α-phase is reached, a new hydride phase, termed β, starts to nucleate, and both phases coexist until total transformation to the β-phase occurs with higher hydrogen pressure. Although for some metals the α- to β-phase transformation is connected to a real structural transformation, Monte Carlo simulations indicate that for Pd clusters, this transformation is associated only with a widening of the Pd lattice [11,12]. It was shown that the surface is first loaded before deeper regions of the clusters are hydrided, with no sign of structural transformation. The Pd–H phase diagram can be divided into two distinct concentration and temperature regimes. At higher temperatures and hydrogen concentrations ≲50%, the only stable phase is a solid solution of hydrogen in Pd, the most stable stoichiometry being a H con-

tent of ~25% at around 566 K. This $PdH_{0.25}$ phase is most likely formed under our experimental conditions, as we discuss in detail below. Crystalline Pd-hydride bulk phases are formed only at hydrogen concentrations >50% and temperatures below 80 K [13].

Pd-hydride formation has been the subject of many studies [14–21] and also may occur during catalytic reactions [10,22]. Because Pd catalysts are used in many reactions involving hydrogen (e.g., hydrogenation of CO [23–27] and of CO_2 [28–31], methanol synthesis [27,28,31]), the presence of Pd hydrides may have a pronounced effect on catalyst performance [10,22]. Pd hydride formation has been reported to either suppress catalytic activity or favor catalytic performance; examples include the enhancement of hydrogenation of alkynes [10] and ethene [32] and the suppression of hydrogenation of cyclohexenes [10]. Altogether, detailed knowledge of the formation of Pd hydrides and of their structural and thermal stability will be of value in understanding the foregoing catalytic processes. A correlation to systems in which hydride formation is excluded under otherwise similar reaction conditions may be particularly helpful. It is known that adding ZnO to a silica-supported Pd catalyst suppresses hydride formation over a wide range of temperatures [33]. This fact has been recently elucidated by the present authors [34], who showed that a topotactic, well-ordered PdZn alloy phase forms on regular Pd nanoparticles under reductive conditions.

The goal of the present contribution is threefold: (i) to understand the mechanism of hydride formation on SiO_2-supported Pd particles, (ii) to prove the structural and thermal stability of the so-obtained hydride phase(s) in both reductive and oxidative environments, and (iii) to test the stability of the Pd/SiO_2 catalyst under "real" reaction conditions. Special emphasis is given to a comparison with the results obtained on a ZnO-promoted Pd/SiO_2 catalyst described previously [34]. To achieve these goals, we exploit the unique properties of well-defined Pd particles grown epitaxially on NaCl(001) supports. These thin-film model systems are known for extended and intimate contact between metal and support and defined particle size and shape, and are therefore especially well-suited for monitoring structural alterations occurring during catalyst activation treatments.

2. Experimental

A high-vacuum chamber (base pressure 10^{-4} Pa) was used to prepare the SiO_2-supported Pd catalysts. Pd metal was deposited by electron-beam evaporation onto a freshly-cleaved NaCl(001) plane at a base pressure of 10^{-4} Pa and a substrate temperature of 623 K. Under these experimental conditions, the deposition of Pd films of about 0.5 nm nominal thickness results in well-shaped Pd particles of about 5 nm in size. Subsequently, the Pd particles were covered by a layer of amorphous SiO_2 (nominal thickness, 25 nm), prepared by reactive deposition of SiO in 10^{-2} Pa O_2 at room temperature. NaCl was subsequently removed by dissolution in distilled water, and after careful rinsing, the resulting thin films were dried and mounted on gold grids for electron microscopy. Subsequently, the films thus prepared were subjected to reductive (1 bar H_2 for 1 h), oxidative

(1 bar O_2 for 1 h), and annealing treatments in parallel in a flow system and a circulating batch reactor in temperature ranges of 373–873 K and 373–573 K, respectively. Structural and morphological changes were followed by high-resolution transmission electron microscopy (HRTEM) and selected area electron diffraction (SAED). The electron micrographs were obtained with a Zeiss EM 10C microscope.

3. Results and discussion

3.1. Hydride formation and stability under reductive conditions

An electron micrograph of the as-deposited Pd/SiO_2 catalyst is shown in Fig. 1a. All structural and morphological alterations occurring during the subsequent reductive, oxidative, or annealing treatments are referenced to this initial state. The Pd particles are visible as dark and gray dots with a mean diameter of ~5.6 nm (see Table 1). A particle density of about 5×10^7 cm^{-2} was estimated by evaluating a number of TEM images from different parts of the sample. Whereas the dark
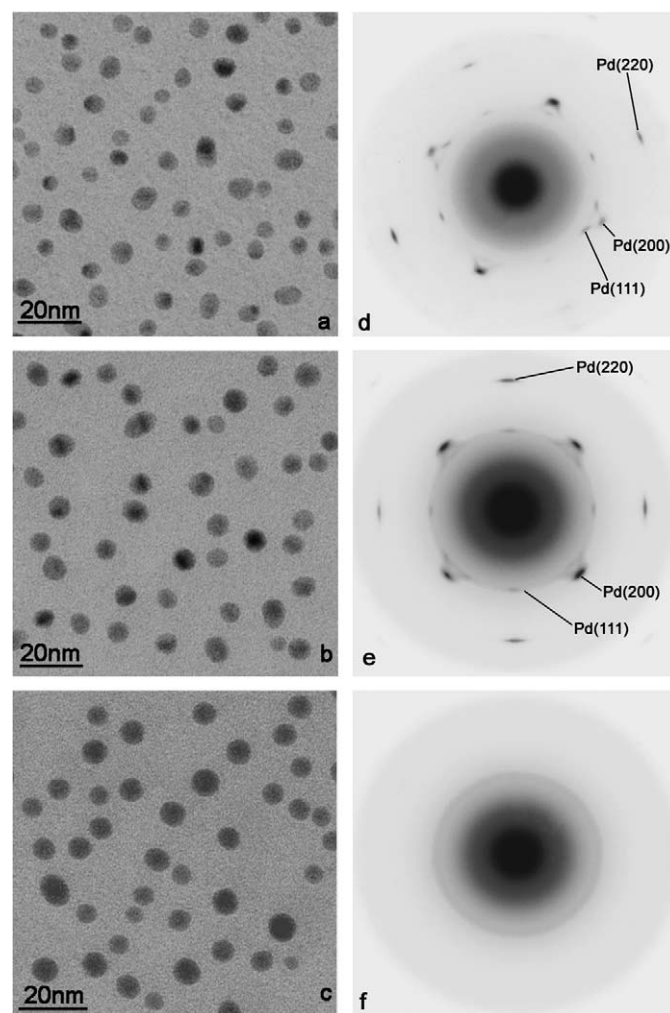

Fig. 1. TEM overview of the Pd–SiO$_2$ catalyst as-deposited (a), and after reduction in 1 bar H$_2$ for 1 h at 473 K (b), and 523 K (c). The corresponding SAED patterns are shown in (d–f).

Table 1
Mean particle diameter of the Pd/SiO$_2$ and Pd/ZnO/SiO$_2$ [34] catalyst after various reductive treatments

Phase	Pd/ZnO/SiO$_2$ as grown	Pd/ZnO/SiO$_2$ 523 K	Pd/ZnO/SiO$_2$ 723 K	Pd/ZnO/SiO$_2$ 873 K
Mean diameter (nm)	5.0	5.3	5.5	5.8
Phase	Pd/SiO$_2$ as grown	Pd/SiO$_2$ 523 K	Pd/SiO$_2$ 673 K	Pd/SiO$_2$ 873 K
Mean diameter (nm)	5.6	6.7	7.4	8.0

particles were perfectly aligned along a Bragg orientation, the gray ones were (slightly) tilted out of their respective Bragg position. A few particles were square or rectangular shaped, but most had more rounded outlines, indicating the presence of higher-indexed facets. Weak-beam dark-field images of the corresponding Al$_2$O$_3$-based Pd thin-film model catalysts reveal their cuboctahedral habit [35]. The SAED patterns (Fig. 1d) show that most Pd particles are oriented along the [001] zone axis. Hence, the most intense reflections are the Pd(200) and Pd(220) spots, measured at $d \approx 1.95$ Å and ≈ 1.37 Å, respectively [at d_{200}(theor) = 1.945 Å and d_{220}(theor) = 1.375 Å]. However, Pd(111) spots are also visible [measured at $d \approx$ 2.25 Å; d_{111}(theor) = 2.245 Å], indicating the presence of a [011] zone axis for some particles. HRTEM images of cuboctahedral particles reveal mainly (200) lattice fringes of the Pd fcc structure [35]; hence, most particles exhibit a (100) plane perpendicular to the electron beam. The SiO$_2$ support is amorphous in the as-grown state and thus contributes no significant contrast to the electron micrographs.

No significant changes in particle structure or morphology were seen on reduction at temperatures below 473 K (in 1 bar hydrogen for 1 h). The state of the catalyst after reduction at 473 K is shown in Fig. 1b. Most particles have adopted more rounded outlines, due to increased formation of higher-indexed facets. The corresponding SAED patterns (Fig. 1e) do not differ significantly from those of the as-grown state or the state observed after reduction at lower temperatures. Only a broadening of the Pd spot reflections points to increased azimuthal disorder. However, massive alterations are introduced if the reduction temperature is raised to 523 K (Fig. 1c). The mean particle diameter is now increased considerably to about 6.7 nm, and SAED patterns (Fig. 1f) consist of only a single diffuse halo, whereas all reflections due to the Pd fcc structure have vanished, indicating that the Pd phase has become almost amorphous. Although nanocrystalline materials are known to be more resistant to hydrogen-induced morphological changes, such as hydrogen-induced decrepitation or amorphization [15], we conclude that this amorphization is due to the formation of a Pd–H phase. As outlined in the Introduction, a solid solution of H in Pd (α-phase) exists at lower hydrogen loadings, and the Pd–H β-phase is formed only at higher hydrogen concentrations and lower temperatures. Recent hydrogen adsorption studies on nanocrystalline Pd samples revealed that the hydrogen uptake was significantly increased compared with bulk material in the solid solution region of the isotherms (i.e., the α-phase), but the maximum hydrogen concentration was considerably lower compared with bulk material in the hydride (β) region. This behavior was attributed to the increased concentration and solubility of hydrogen at the grain boundaries, but
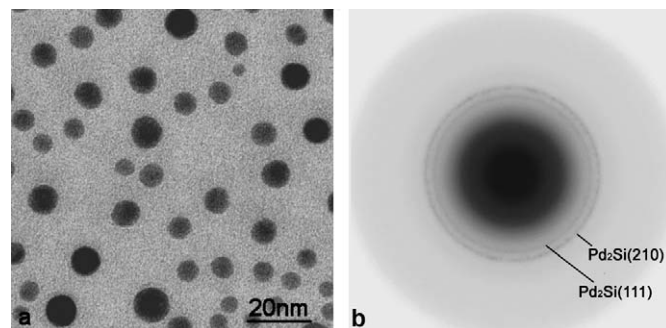

Fig. 2. The Pd–SiO$_2$ catalyst after reduction in 1 bar H$_2$ for 1 h at 673 K (a) with the corresponding SAED pattern (b).

without transformation of these into the hydride β-phase [15]. Hence, we propose that the observed behavior on Pd/SiO$_2$ can be interpreted in terms of an accumulation of hydrogen at surface and interface sites, forming an amorphous solid solution (α-phase) on penetrating the Pd particles, and that the whole particles are transformed exclusively into the α-phase, as confirmed by the absence of Pd reflections and signs of any other crystalline phase in the SAED patterns.

Fig. 2a shows the state of the catalyst after a reduction at 673 K in 1 bar H$_2$ for 1 h. Compared with the reduction at 523 K, the mean particle size again has increased considerably, to ~7.5 nm, pointing to enhanced material uptake into the Pd bulk at elevated temperature. Although no indications of changes in the particle structure can be seen in the TEM micrographs, the corresponding SAED pattern (Fig. 2b) indicates at least partial recrystallization. Two rather blurred Debye–Scherrer-type ring reflections are seen, corresponding to lattice distances of ~2.31 Å and ~2.10 Å. These reflections were also observed previously [35] in the Pd/ZnO/SiO$_2$ system after reduction at and above 873 K and can be attributed to the (111) and (210) reflections of the hexagonal Pd$_2$Si structure (space group P-62m, $a = b = 6.49$ Å, $c = 3.42$ Å) [d_{111}(theor) = 2.35 Å and d_{210}(theor) = 2.12 Å] [36].

A further increase of the reduction temperature to 873 K did not significantly alter either the particle morphology or the SAED patterns (not shown here). The mean particle size increased to approximately 8 nm, and the electron diffraction pattern exhibited only reflections of the above-mentioned Pd$_2$Si structure. No other species besides Pd$_2$Si were present in detectable concentrations. This implies that the hydride phase decomposed at least partially on reduction at and above 673 K, accompanied by silicide formation, whereas the Pd$_2$Si phase exhibited a broad stability range up to 873 K. These results are further corroborated by recently published HRTEM images of highly oriented single-crystalline Pd$_2$Si particles [34].
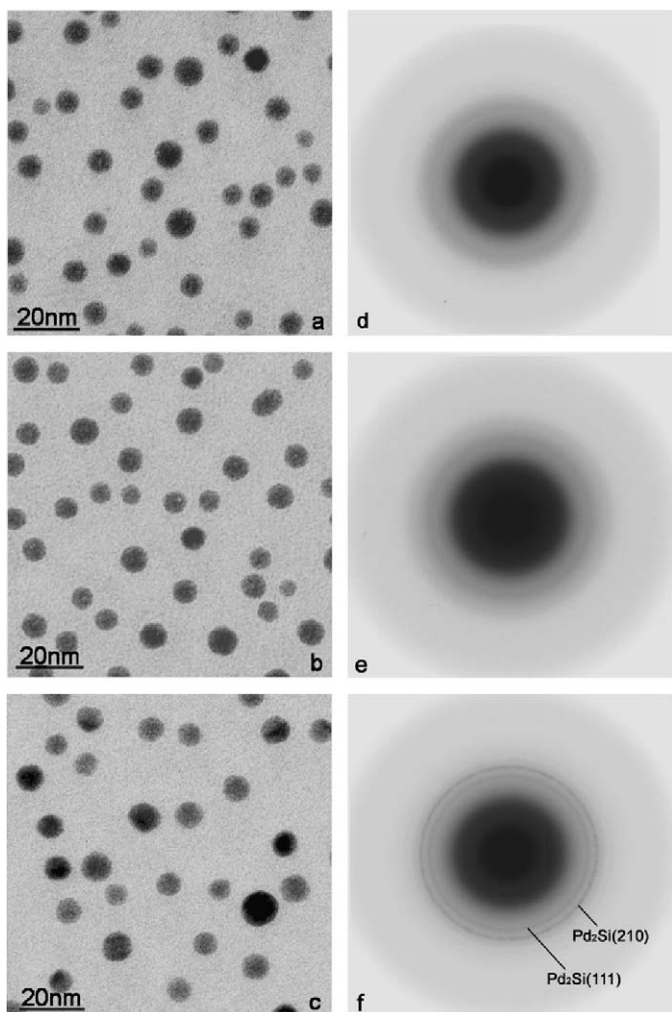
Fig. 3. State of the Pd/SiO$_2$ catalyst after reduction in 1 bar H$_2$ at 523 K for 1 h, followed by annealing in He at 523 K for 16 h (a), at 573 K for 1 h (b), and at 673 K for 1 h (c). The corresponding SAED patterns are shown in (d–f).

3.2. Thermal stability of the hydride

The question arises as to whether the amorphous α-hydride is destroyed only by reduction at increasing temperature, leading to silicide formation, or whether annealing treatments in He or oxidation at elevated temperatures ultimately lead to the same result. Fig. 3a shows the state of the catalyst after a 16-h treatment in 1 bar He at 523 K. No change in particle morphology can be seen, and the SAED pattern (Fig. 3d) still exhibits the halos characteristic of an amorphous sample. Further raising the annealing temperature to 573 K (1 bar He for 1 h) did not alter the amorphous state of the catalyst, as can be deduced from Fig. 3b (TEM overview image) and Fig. 3e (SAED pattern). However, annealing the sample in 1 bar He at 673 K for 1 h caused an increase in mean particle size compared with the state after reduction at 573 K, with partial recrystallization indicated by the formation of sharp internal grain boundaries for some particles (Fig. 3c). These observations are augmented by SAED patterns (Fig. 3f) showing reflections of a crystalline sample. An analysis of the reflections measured at ~2.33 Å and ~2.10 Å reveals the hexagonal Pd$_2$Si struc-
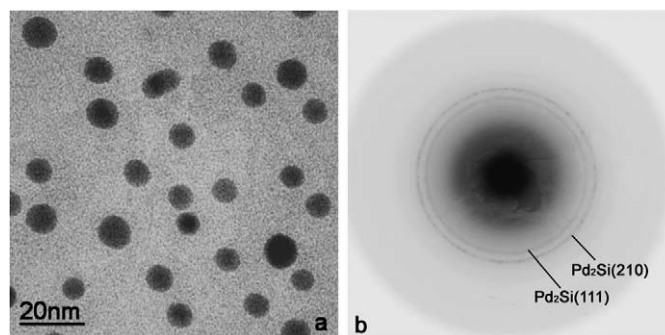

Fig. 4. (a) Overview electron micrograph of the Pd/SiO$_2$ catalyst after annealing in 1 bar He at 673 K for 1 h, followed by reduction in 1 bar H$_2$ at 523 K for 1 h. The corresponding SAED pattern is shown in (b).

ture already observed after reducing the hydride phase in hydrogen at 673 K and above. Alloy formation under reductive conditions is thermodynamically feasible and has been shown to occur on similar thin-film catalysts (Pt/SiO$_2$ [37], Pt/CeO$_2$ [38], Rh/VO$_x$ [39]) on reduction at elevated temperatures. The fact that Pd$_2$Si forms at the same temperature after reduction in hydrogen and after annealing in He indicates that its formation becomes kinetically feasible at 673 K if reoxidation of the intermetallic compound is suppressed by the experimental conditions.

Can the Pd$_2$Si alloy reconvert to the α-hydride phase? The Pd/SiO$_2$ catalyst was annealed at 673 K in 1 bar He for 1 h, and the resulting Pd$_2$Si alloy was subsequently reduced in hydrogen at 523 K. Fig. 4a shows the catalyst after this hydrogen treatment. Obviously, the catalyst morphology was not significantly altered compared with that observed after the previous annealing treatment in He, and the SAED pattern (Fig. 4b) still shows the Pd$_2$Si (111) and (210) ring reflections (cf. Figs. 3c and f). Hence, after entering the silicide state, Pd loses its hydrogen storage capability, and the hydride state cannot be reestablished by hydrogen treatments at even higher temperatures.

3.3. Hydride stability under oxidative conditions

The stability of the Pd-hydride phase in an oxidizing environment was checked and compared with that of the silicide phase treated under identical experimental conditions. The hydride phase was again prepared by reducing the Pd/SiO$_2$ catalyst at 523 K, and the silicide phase was obtained by annealing in He at 673 K, as outlined above. Subsequently, both systems were annealed simultaneously in 1 bar O$_2$ in 50-K steps in the temperature range of 373–623 K. On oxidation at below 473 K, no changes were detected in either system. Figs. 5a and c show the Pd$_2$Si phase and the Pd–H phase after oxidation at 473 K, and Figs. 5b and d show the corresponding SAED patterns. The silicide particles in Fig. 5a are slightly larger than the hydride particles in Fig. 5c. Fig. 5b still exhibits the Debye–Scherrer-type ring reflections of the Pd$_2$Si alloy. Some particles in Fig. 5c already exhibit an internal grain boundary pointing to the start of recrystallization of the hydride phase, which is further confirmed by the weakly visible Pd(111) reflection detected in the corresponding SAED pattern (Fig. 5d).
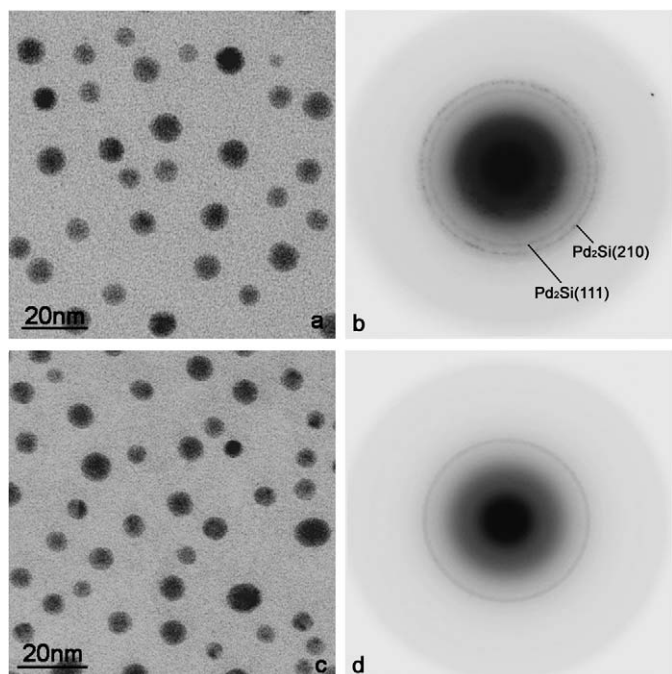
Fig. 5. (a) TEM overview of the Pd/SiO$_2$ catalyst after annealing in 1 bar He at 673 K for 1 h, followed by oxidation in 1 bar O$_2$ at 473 K. (b) Corresponding SAED pattern. (c) Overview of the Pd/SiO$_2$ catalyst after reduction at 523 K in 1 bar H$_2$ for 1 h, followed by oxidation in 1 bar O$_2$ at 473 K. (d) Corresponding SAED pattern.
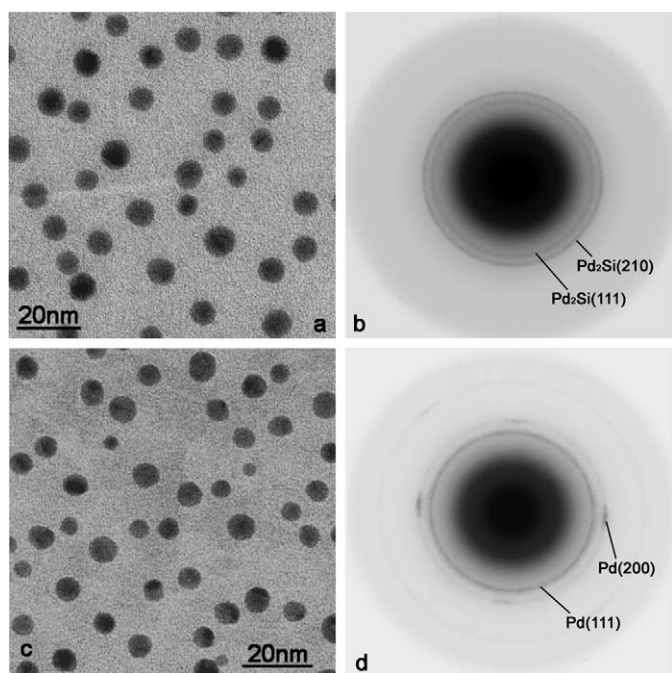

Fig. 7. (a) TEM overview of the Pd/SiO$_2$ catalyst after annealing in 1 bar He at 673 K for 1 h, followed by oxidation in 1 bar O$_2$ at 573 K. (b) Corresponding SAED pattern. (c) Overview of the Pd/SiO$_2$ catalyst after reduction at 523 K in 1 bar H$_2$ for 1 h, followed by oxidation in 1 bar O$_2$ at 573 K. (d) Corresponding SAED pattern.

Fig. 6. (a) TEM overview of the Pd/SiO$_2$ catalyst after annealing in 1 bar He at 673 K for 1 h followed by oxidation in 1 bar O$_2$ at 523 K. (b) Corresponding SAED pattern. (c) TEM overview of the Pd/SiO$_2$ catalyst after reduction in 1 bar H$_2$ at 523 K followed by oxidation in 1 bar O$_2$ at 523 K. (d) Corresponding SAED pattern.

On raising the oxidation temperature to 523 K, the Pd$_2$Si alloy persists, and no structural alterations are evident (Figs. 6a and b). However, as shown in Fig. 6c, some of the former hy-
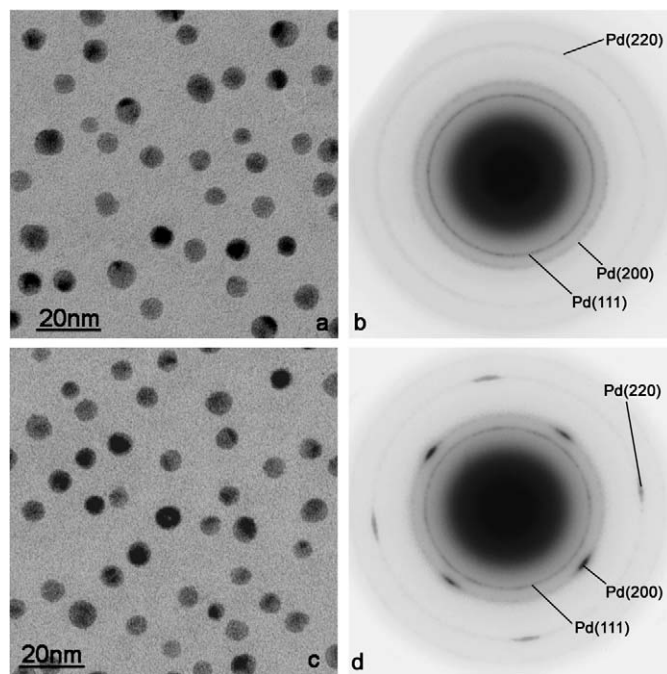
dride particles have adopted straight edges, further corroborating the partial recrystallization already observed at a temperature 50 K lower. The corresponding SAED pattern in Fig. 6d indicates the presence of a partially ordered structure. Three strong reflections appear at ∼2.24, 1.95, and 1.37 Å, in agreement with the fcc lattice spacings of Pd(111), Pd(200), and Pd(220). The Pd(200) and Pd(220) reflections appear as broad spots superimposed on the respective Debye–Scherrer rings. This implies that the hydride has decomposed and that the Pd particles have at least partially returned to their previous oriented alignment. This behavior allows some conclusions concerning hydride formation. The fact that the previous epitaxial Pd structure is partly reestablished after hydride decomposition indicates that the hydride phase into which the Pd particles were converted must have some structural relationship to the former Pd lattice. Otherwise, the Pd particles would have lost their alignment with respect to the supporting silica film and would not have been able to readopt this epitaxial orientation once the new phase was once again destroyed. Hence it is reasonable to assume that hydrogen is bound primarily at surface and interface sites and finally spreads within the Pd lattice, forming a solid solution of α-phase type. This process of spreading and dilution will not lead to *complete* recrystallization of the Pd lattice, and hence the particles can regain their initial crystallographic orientation on decomposition without the need for long-range mass transport. This picture is corroborated by the results obtained after further raising the oxidation temperature to 573 K. Fig. 7a shows that after this treatment, the Pd–Si alloy particles appear smaller and partly recrystallized, with some exhibiting pronounced edges in various directions. The SAED
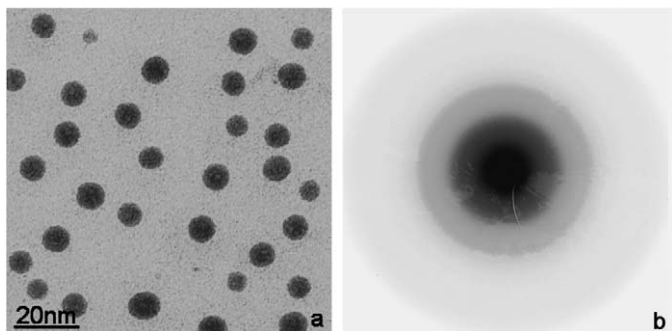
Fig. 8. (a) TEM overview of the Pd/SiO$_2$ catalyst after exposition to a reaction mixture of 200 mbar CO$_2$ and 800 mbar H$_2$ at 523 K for 1 h. (b) Corresponding SAED pattern.

pattern (Fig. 7b) reveals that at this temperature the Pd$_2$Si phase also has decomposed, but now only Pd(111), (200), and (220) ring reflections with no particular orientation are obtained, in distinct contrast to the decomposition of the hydride phase (cf. Fig. 6d). Because the Pd$_2$Si phase does not exhibit a crystallographic relationship relative to the original Pd lattice, topotactic silicide formation is basically excluded; the particle structure is altered and leads to a random change in orientation, which cannot be reestablished after decomposition of the silicide phase (because the particles have "lost their memory"). In contrast, the state of the former hydride phase after oxidation at 573 K is characterized by rather small particles (Fig. 7c), and the SAED pattern (Fig. 7d) shows improved ordering of the Pd particles compared with the state after 523 K (Fig. 6d), with more intense but still broadened Pd(200) and Pd(220) spot reflections superimposed on the Debye–Scherrer rings. It is also noteworthy that oxidative decomposition of the hydride and the Pd$_2$Si phase differs by about 50 K, further underscoring the different properties of the two phases.

3.4. Implications of hydride formation for catalysis

The final question addresses possible implications of hydride formation for catalysis. In close correlation with the studies on the corresponding Pd/ZnO/SiO$_2$ catalyst [34], which is an excellent catalyst for methanol synthesis and methanol steam reforming and involves the presence of a PdZn alloy phase, we focused on the state of the Pd/silica catalyst under typical reaction conditions of CO$_2$ hydrogenation. The catalyst was treated in a reaction mixture of 200 mbar CO$_2$ and 800 mbar H$_2$ at 523 K for 1 h, and the resulting structure was examined. The results are shown in Figs. 8a and b. The close relationship to Figs. 1c and f is immediately apparent. The particles have considerably increased in size, and the SAED pattern shows only an amorphous state of Pd. Hence, even under typical CO$_2$ hydrogenation conditions, a Pd hydride phase is formed.

3.5. Correlation with results obtained on a Pd/ZnO/SiO$_2$ catalyst

At this stage, it is useful to compare this state of the Pd/SiO$_2$ catalyst with the observations on a ZnO-promoted Pd/SiO$_2$ cat-

alyst treated under similar experimental conditions [34]. In this case, after reduction at 523 K, the formation of a well-defined PdZn alloy phase was observed instead of the amorphous state of the Pd particles. Furthermore, this alloy formation occurred with only a minor increase in the mean particle diameter, to ∼5.3 nm. This means that adding ZnO to the Pd/SiO$_2$ catalyst structurally stabilized the Pd particles by alloy formation and prevented their amorphization.

It is also noteworthy that in this system, a Pd$_2$Si phase was also formed on reduction, but only at much higher temperature ($\geqslant$873 K), and that even at this high temperature, the predominant PdZn alloy was only partially destroyed. In contrast, on the Pd/SiO$_2$ catalyst, the Pd$_2$Si phase was the dominant species already on reduction at 673 K and above. Moreover, the ZnO-promoted catalyst (in the PdZn alloy state) did not undergo hydride formation under realistic hydrogenation conditions.

4. Conclusion

The main conclusions from this work can be summarized as follows. Under the given conditions (1 bar H$_2$), hydride formation on Pd particles supported on SiO$_2$ occurs at rather low temperatures (523 K), resulting in an amorphous structure ascribed to a solid solution of H in the Pd lattice (α-phase). The maximum stability of this phase is at $T = 566$ K and at $x_{H_2} = 22.5\%$, as deduced from the Pd–H diagram [13]. This hydride appears to be very stable on both reductive treatment and annealing in He atmosphere and decomposes after either of these treatments at 673 K through formation of a crystalline Pd$_2$Si phase. Pd particles in their "previous" orientational alignment are obtained after oxidative decomposition of the hydride phase at and above 523 K. A treatment under typical reaction conditions for CO$_2$ hydrogenation results in the same amorphous hydride phase, strongly suggesting that hydride formation should be considered whenever mechanisms for reactions involving hydrogen (e.g., CO and CO$_2$ hydrogenation, methanol synthesis) over supported Pd catalysts are discussed. The Pd particles supported on SiO$_2$ lose their hydrogen storage capability once the Pd$_2$Si phase is formed. An overview of the different reaction pathways of Pd particles supported on SiO$_2$ is given in Scheme 1.

Finally, our results stand in striking contrast to previous findings on a related ZnO-promoted Pd/SiO$_2$ catalyst [34]. In the latter case, in the same temperature range the formation of a topotactic PdZn alloy prevented hydride formation and structurally stabilized the Pd particles against sintering at temperatures up to 900 K. In contrast, in our work the pure Pd/SiO$_2$ catalyst is structurally less stable and prone to sintering and silicide formation at temperatures at and above 523 K, eventually resulting in Pd$_2$Si alloy formation at temperatures 200 degrees lower than for the ZnO-promoted catalyst (PdZn alloy state). Therefore, our results on the behavior of SiO$_2$-supported Pd particles and the differences from the Pd/ZnO/SiO$_2$ system provide important information concerning the functional performance of the latter catalyst in methanol synthesis and steam reforming.
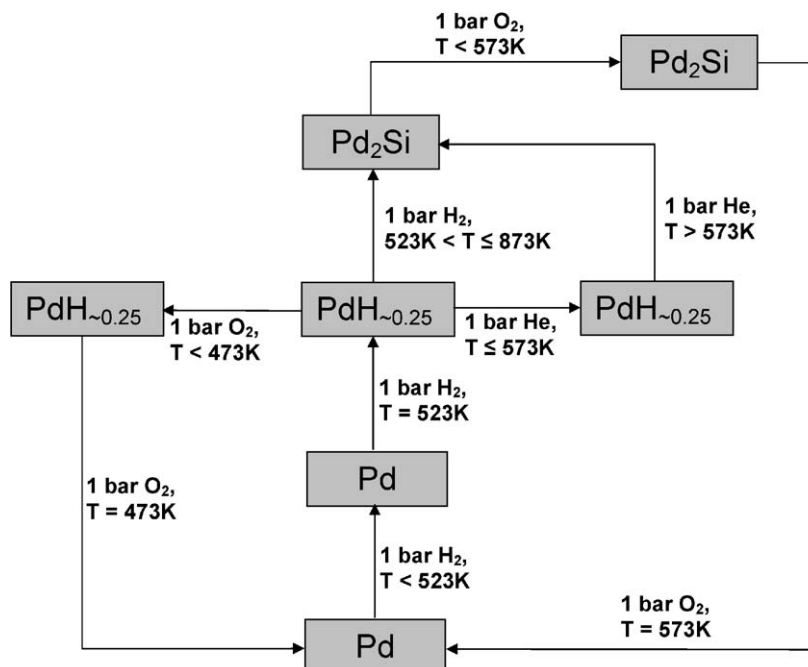
Scheme 1. Reaction scheme of different treatments of the Pd/SiO$_2$ catalyst.

Acknowledgments

References

[1] T. Graham, Phil. Trans. Roy. Soc. London 156 (1866) 4151.

[2] F.A. Lewis, The Palladium Hydrogen System, Academic Press, London, 1967.

[3] L. Zaluski, A. Zaluska, P. Tessier, J.O. Ström-Olsen, R. Schulz, J. Alloys Compd. 217 (1995) 295.

[4] Z. Dehouche, R. Djaozandri, J. Huot, S. Boily, J. Goyette, T.K. Bose, R. Schulz, J. Alloys Compd. 305 (2000) 264.

[5] Z. Dehouche, R. Djaozandri, J. Goyette, T.K. Bose, J. Alloys Compd. 288 (1999) 312.

[6] S. Orimo, H. Fujii, K. Ikeda, Y. Fujikama, Y. Kitano, J. Alloys Compd. 253–254 (1997) 94.

[7] T. Saito, K. Suwa, T. Kawamura, J. Alloys Compd. 253–254 (1997) 682.

[8] G. Liang, S. Boily, J. Huot, A. Van Neste, R. Schulz, J. Alloys Compd. 267 (1998) 302.

[9] L. Zaluski, A. Zaluska, H.O. Ström-Olsen, J. Alloys Compd. 253–254 (1997) 70.

[10] W.F. Maier, in: P.N. Nylander, H. Greenfield, A.L. Augustine (Eds.), Catalysis of Organic Reactions, Marcel Dekker, New York, 1988.

[11] R.J. Wolf, M.W. Lee, J.R. Ray, Phys. Rev. Lett. 73 (1994) 557.

[12] R.J. Wolf, M.W. Lee, R.C. Davis, P.J. Fay, J.R. Ray, Phys. Rev. B 48 (1993) 12415.

[13] Phase Equilibria, Crystallographic and Thermodynamic Data of Binary Alloys, Landolt–Börnstein New Series, vol. 5, Springer, Berlin, 1998.

[14] G. Fagherazzi, A. Benedetti, S. Polizzi, A. DiMario, F. Pinna, M. Signoretta, N. Pernicone, Catal. Lett. 32 (1995) 293.

[15] S. Kishore, J.A. Nelson, J.H. Adair, P.C. Eklund, J. Alloys Compd. 389 (2005) 234;
C. Sachs, A. Pundt, R. Kirchheim, M. Winter, M.T. Reetz, D. Fritsch, Phys. Rev. B 64 (2001) 075408.

[16] R.W. Wunder, J.W. Cobes, J. Phillips, L.R. Radovic, A.J. Lopez Peinado, F. Carrasco-Marin, Langmuir 9 (1993) 984.

[17] A. Pundt, C. Sachs, M. Winter, M.T. Reetz, D. Fritsch, R. Kirchheim, J. Alloys Compd. 293–295 (1999) 480.

[18] J.A. Eastman, L.J. Thompson, B.J. Kestel, Phys. Rev. B 48 (1993) 84.

[19] M. Boudart, H.S. Hwang, J. Catal. 39 (1995) 44.

[20] R. Dus, R. Nowakowski, E. Nowicka, J. Alloys Compd. 404–406 (2005) 284.

[21] N.K. Nag, J. Phys. Chem. B 105 (2001) 5945.

[22] W. Palczewka, in: Z. Paál, P.G. Menon (Eds.), Hydrogen Effects in Catalysis, Marcel Dekker, New York, 1988.

[23] P.C. Aben, J. Catal. 10 (1968) 224.

[24] W. Shen, M. Okumura, Y. Matsumura, M. Haruta, Appl. Catal. A 213 (2001) 225.

[25] R.F. Hicks, A.T. Bell, J. Catal. 91 (1985) 104.

[26] Y. Borodko, G.A. Somorjai, Appl. Catal. A 186 (1999) 355.

[27] M.L. Poutsma, L.F. Elek, P.A. Ibarbia, A.P. Risch, J.A. Rabo, J. Catal. 52 (1978) 157.

[28] L. Fan, K. Fujimoto, J. Catal. 150 (1994) 217.

[29] A.L. Bonivardi, D.L. Chiavassa, C.A. Querini, M.A. Baltanas, Stud. Surf. Sci. Catal. 130 (2000) 3747.

[30] A. Erdöhelyi, M. Pasztor, F. Solymosi, J. Catal. 98 (1986) 166.

[31] T. Fujitani, M. Saito, Y. Kanai, T. Watanabe, J. Nakamura, T. Uchijima, Appl. Catal. A 125 (1995) L199.

[32] M. Morkel, G. Rupprechter, H.-J. Freund, Surf. Sci. Lett. 588 (2005) L209.

[33] N. Iwasa, T. Manyagi, N. Ogawa, K. Sakata, N. Takezawa, Catal. Lett. 54 (1998) 119.

[34] S. Penner, B. Jenewein, H. Gabasch, B. Klötzer, D. Wang, A. Knop-Gericke, R. Schlögl, K. Hayek, J. Catal., in press, doi:10.1016/j.jcat.2006.04.005.

[35] G. Rupprechter, K. Hayek, L. Rendón, J.-M. Yacamán, Thin Solid Films 260 (1995) 148.

[36] G. Anderko, H. Schubert, Z. Metallkd. 44 (1953) 307.

[37] D. Wang, S. Penner, D.S. Su, G. Rupprechter, K. Hayek, R. Schlögl, J. Catal. 219 (2003) 434.

[38] S. Penner, D. Wang, R. Podloucky, R. Schlögl, K. Hayek, Phys. Chem. Chem. Phys. 6 (2004) 5244.

[39] S. Penner, B. Jenewein, D. Wang, R. Schlögl, K. Hayek, Phys. Chem. Chem. Phys. 8 (10) (2006) 1223.